The quantitative landscape of the neutralizing antibody response to SARS-CoV-2

Pranesh Padmanabhan[1,*], Rajat Desikan[2,‡], Narendra M. Dixit[2,3,*]

[1]Clem Jones Centre for Ageing Dementia Research, Queensland Brain Institute, The University of Queensland, Brisbane, Australia 4072

[2]Department of Chemical Engineering, Indian Institute of Science, Bangalore, India 560012

[3]Centre for Biosystems Science and Engineering, Indian Institute of Science, Bangalore, India 560012

[‡]Current Address: Certara QSP, Certara UK Limited, Sheffield, UK

[*]Correspondence:

Pranesh Padmanabhan, Narendra M. Dixit

Email: p.padmanabhan@uq.edu.au; narendra@iisc.ac.in

Manuscript details:

Abstract: 150 words; Text: ~3300 words; Figures: 6; References: 51

Supplementary Materials: Tables: 1; Figures: 9; References: 20

Abstract

Neutralizing antibodies (NAbs) appear promising interventions against SARS-CoV-2 infection. Over 100 NAbs have been identified so far and several are in clinical trials. Yet, which NAbs would be the most potent remains unclear. Here, we analysed reported *in vitro* dose-response curves (DRCs) of >70 NAbs and estimated corresponding 50% inhibitory concentrations, slope parameters, and instantaneous inhibitory potentials (*IIPs*), presenting a comprehensive quantitative landscape of NAb responses to SARS-CoV-2. NAbs with high *IIPs* are likely to be potent. To assess the applicability of the landscape *in vivo*, we analysed available DRCs of NAbs from individual patients and found that the responses closely resembled the landscape. Further, we created virtual patient plasma samples by randomly sampling NAbs from the landscape and found that they recapitulated plasma dilution assays from convalescent patients. The landscape thus offers a facile tool for benchmarking NAbs and would aid the development of NAb-based therapies for SARS-CoV-2 infection.

Introduction

The pace of the development of neutralizing antibodies (NAbs) against the severe acute respiratory syndrome coronavirus 2 (SARS-CoV-2) has been phenomenal[1]. Over 100 monoclonal NAbs have been identified so far and several of them, namely, LY-CoV555, JS016, REGN10933/10987, VIR-7831/7832, TY027, SCTA01, BRII-196/198, CT-P59, AZD8895/1061 and MW33 are already in clinical trials[2,3]. Drugs and vaccines specifically targeting SARS-CoV-2 are not yet available. Plasma therapy, where plasma isolated from convalescent patients is injected into infected individuals, has shown some success and is in use in some countries to treat severe SARS-CoV-2 infection[4-6]. The reported NAbs have been isolated from convalescent patients and subsequently selected or engineered for improved potency[1,2], and are therefore expected to work better than plasma therapy[7]. NAbs thus hold promise of evolving into a powerful weapon against SARS-CoV-2 infection. Passive immunization with antibodies has shown promise in several other settings, including HIV-1 infection[8,9], autoimmune disorders[10,11], and cancers[12,13]. With the large and rapidly growing SARS-CoV-2 NAb repertoire, a question that arises is which of these NAbs should be taken up for clinical development. A comparative evaluation of the NAbs has not been performed.

Studies identifying NAbs typically report the 50% inhibitory concentration, IC_{50}, of the NAbs, the concentration at which viral infectivity is reduced by 50% of that in the absence of the NAbs (Fig. 1A). The inference drawn is that the lower is the IC_{50}, the more potent is the NAb (Fig. 1A). A limitation of this approach arises from the non-linear dependence of the neutralization efficacy of NAbs on their concentrations because of which a NAb with a lower

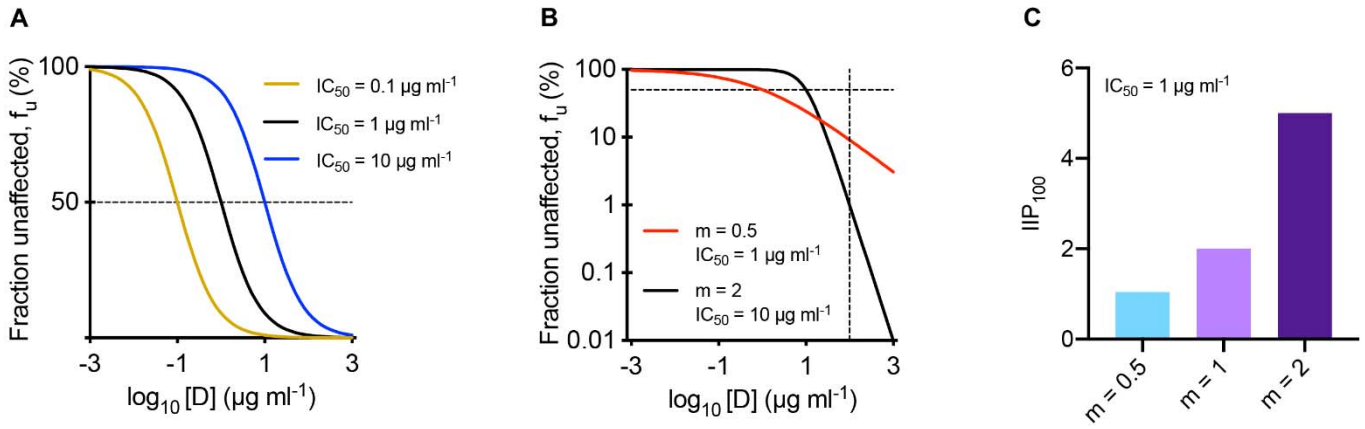

Figure 1. Illustration of assays and metrics characterizing NAbs. (A, B) The fraction of infection events unaffected by NAbs, f_u, with the same m and different values of IC_{50} (A) and with different values of m and IC_{50} (B). In A and B, horizontal lines mark f_u = 50%. In B, vertical line marks NAb concentration, D, of 100 μg/ml. (C) IIP computed at 100 μg/ml for NAbs with the same IC_{50} but different values of m.

IC_{50} may be much less efficacious than a NAb with a higher IC_{50} when the two are used at physiologically relevant concentrations, which are typically much larger than IC_{50} (Fig. 1B). This problem was first recognized with antiretroviral drugs[14-17]. It was overcome by the construction and use of a metric called the instantaneous inhibitory potential, denoted IIP, which is a composite of the IC_{50} and the slope of the dose-response curve (DRC), m, the latter a measure of the extent of the non-linearity in the dependence of the efficacy on the concentration. $IIP = \log_{10}\left(1+\left(\frac{D}{IC_{50}}\right)^{m}\right)$ is the log decline of viremia in a single round infection assay due to the drug at concentration D. Thus, when two drugs are used at the same concentration, the one with the higher IIP would be more efficacious (Fig. 1C). Drug combinations with higher IIP values have been shown to have better efficacies, with HIV-

1[14,15] and hepatitis C virus (HCV)[18,19]. *IIP* has since been extended to antibodies and shown to predict the relative efficacies of HIV-1 and HCV antibodies[18,20].

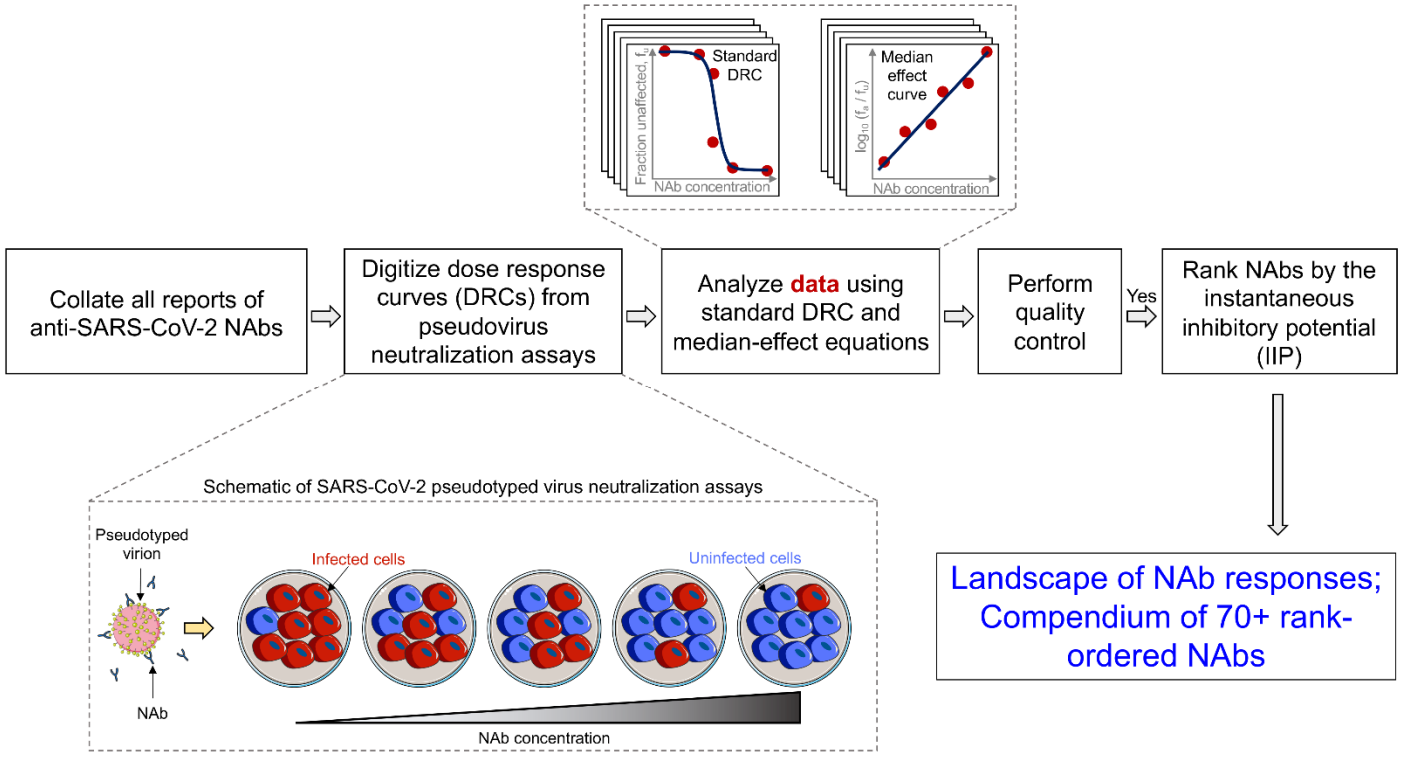

Figure 2. Schematic of the workflow to chart out the quantitative landscape of SARS-CoV-2 NAbs. We collated data from all studies that reported DRCs of NAbs using SARS-CoV-2 pseudotyped virions. The assays estimate the fraction of infection events affected/unaffected by the NAbs as a function of the NAb concentration. We extracted and analysed the data using both the standard DRC equation (Eq. [1]) and the median-effect equation (Eq. [2]) to estimate IC_{50} and m. We then computed $IIP_{100} = \log_{10}\left(1+\left(\frac{100}{IC_{50}}\right)^{m}\right)$ using the estimates obtained by both equations. NAbs with consistent estimates were considered for rank-ordering.

Here, we decided to examine whether the *IIP* could be applied to comparatively evaluate SARS-CoV-2 NAbs. Unlike IC_{50} values, which are routinely reported, the values of

m have rarely been reported for SARS-CoV-2 NAbs, precluding the estimation of *IIP* for most NAbs. We therefore collated all the available *in vitro* DRCs of SARS-CoV-2 NAbs and analysed them to estimate both IC_{50} and *m*, and then *IIP* (Fig. 2). A comprehensive landscape of NAb responses to SARS-CoV-2 emerged. We tested the applicability of the landscape *in vivo* by examining the spectrum of responses in individual patients and by constructing virtual patient plasma samples to recapitulate plasma dilution assays.

Results

Analysis of DRCs and the variability in IC_{50} and m

We collated and analysed the reported DRCs of over 70 NAbs obtained using SARS-CoV-2 pseudotyped virus infection assays (Figs. 2 and 3; Methods; Table S1)[21-39]. These NAbs have been proposed as the most promising from among many examined in the respective studies. A vast majority of the DRCs could be fit well with the median effect equation (Fig. 3A; Fig. S1) as well as the standard dose-response equation (Fig. 3B; Fig. S2), with the two yielding very similar estimates of the fit parameters IC_{50} and *m* (Table S1). The resulting estimates of IC_{50} were in close agreement with the reported estimates, giving us confidence in the fits (Fig. S3A; Table S1). The IC_{50} displayed a wide variation across NAbs, ranging from ~10^{-3} µg/ml to ~140 µg/ml (Fig. 3C). *m* too displayed wide variability, spanning the range ~0.2 to 2.3 (Fig. 3D). As mentioned above, values of *m* have not been reported in previous studies. We examined whether the variability in IC_{50} and *m* was restricted to a particular pseudotyped virus construct or backbone used (Fig. 3F, 3G), the cell line used (Fig. 3H, 3I), or assay conditions, which could vary across studies (Fig. S3B, S3C), and found that not to be true.

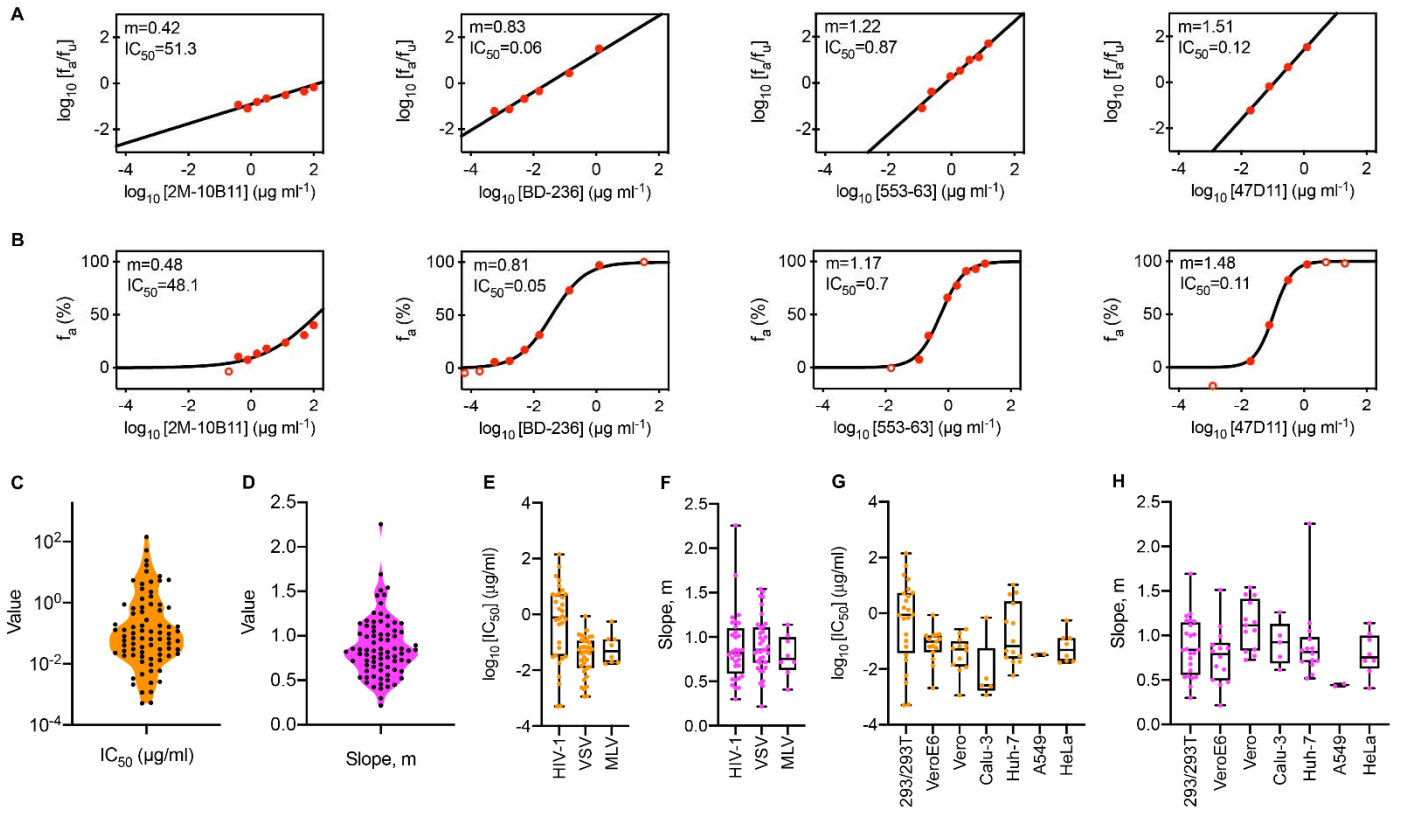

Figure 3. Estimates of IC_{50} and m of SARS-CoV-2 NAbs. (A, B) Fits (lines) of the median-effect equation (A) and the standard dose-response curve equation (B) to published experimental data (circles). The unit of IC_{50} is μg/ml. Experimental data points with 1% < f_u < 99% (filled circles) were considered for parameter estimation. (C, D) The best-fit estimates of IC_{50} (C) and m (D). (E-H) The variability in IC_{50} and m within different pseudotyped virus constructs or backbones (E, F) and cell lines (G, H). In G and H, 293, 293T, HeLa and A549 cells expressing ACE2 were used in the reported experiments.

The variation was thus intrinsic to the NAbs. Furthermore, akin to HIV-1 antibodies[20], the variations in IC_{50} and m of the SARS-CoV-2 NAbs appeared independent. For instance, the NAbs BD-361 and REGN10954 had similar IC_{50} (both ~0.04 μg/ml), but vastly different m (~0.7 and ~1.5, respectively), whereas the NAbs CC12.3 and 515-5 had vastly different IC_{50} (~0.02 μg/ml and 1.6 μg/ml, respectively), but similar m (both ~1). This independent variability of IC_{50} and m implied that IC_{50} alone was an inadequate metric to characterize the NAbs. Indeed, at concentrations of 10×IC_{50}, REGN10954 would have an efficacy of ~0.97

and therefore perform better than BD-361, which would have an efficacy ~0.84, despite the two having similar values of the IC_{50}.

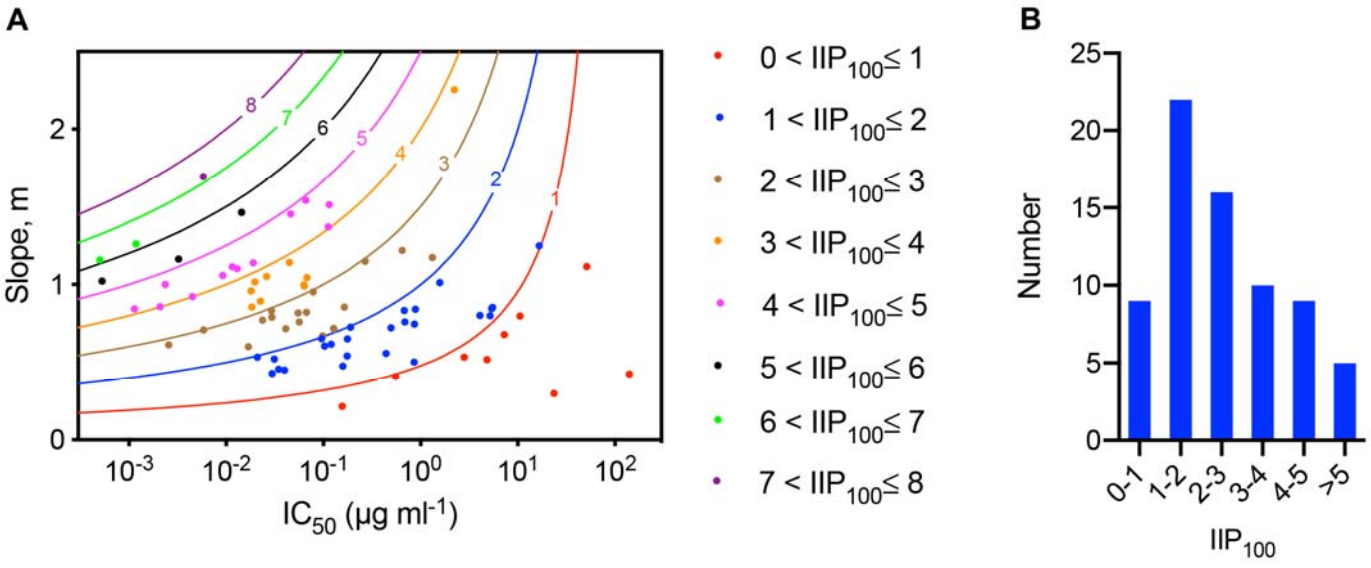

Figure 4. The SARS-CoV-2 NAb landscape. (A) IC_{50} and m for SARS-CoV-2 NAbs (circles colour-coded with the respective *IIP* values computed at 100 μg/ml). Each symbol represents one NAb. 8 NAbs that have multiple neutralisation curves reported are represented multiple times (Table S1). Lines are loci of points corresponding to fixed *IIP* values computed at 100 μg/ml. (B) The distribution of IIP_{100} values of NAbs. Average IIP_{100} values are used for the 8 NAbs mentioned above.

IIP estimates, the NAb landscape, and benchmarks

Following previous studies on HIV-1 and HCV[18-20], we therefore computed next the *IIP* values of the NAbs at D=100 μg/ml. We found that the *IIP* displayed a wide range, from ~0.3 to 7.2 (Figs. 4 and 5), giving a glimpse of the range of NAb efficacies realizable *in vivo*. (*IIP* values at D = 50 μg/ml displayed negligible deviations in the rank-ordering of the NAbs; Fig. S4). NAbs with high *IIPs* were those with low IC_{50} and high m (Fig. 4A). Contour lines of constant *IIP* on an IC_{50}–m plot helped visualize the dependence of the *IIP* on IC_{50} and m

(Fig. 4A). We found that 5 NAbs had *IIP* > 5. These, from our calculations, would be the most promising NAbs. (Similar predictions have been made with broadly neutralizing antibodies of HIV-1[20].) The numbers increased for smaller *IIP*, with 9 NAbs between 4 and 5, 10 between 3 and 4, and so on (Fig. 4B). The highest number, 22, had modest *IIPs*, between 1 and 2. A much smaller number, 9, had *IIPs* between 0 and 1, which was predictive of poor *in vivo* efficacy.

This distribution of *IIP* values demonstrates the wide spectrum of neutralization efficiencies of NAbs that have all been deemed promising in different studies. The threshold *IIP* for clinical success is not known. While many NAbs with low *IIPs* may thus prove successful, it may be advantageous to choose those with high *IIPs* for they are likely to succeed with smaller dosages and/or fewer doses than those with low *IIPs*. Based on the resources available, thus, the top few NAbs, *i.e.*, those with the highest *IIP* values (Fig. 5), could be considered for further development. We note that the top NAbs would have been different had the IC_{50} or *m* alone been used to characterize the NAbs, reiterating the inadequacy of these metrics individually in characterizing NAbs. (Figs. S5 and S6). The range of *IIPs* we estimated also sets benchmarks for NAbs that may be discovered/engineered in the future. They are unlikely to be competitive if they have *IIP* < 5 and more certainly so with *IIP* < 4.

NAb responses in patients

An important question in choosing NAbs based on our analysis above is the applicability of the landscape to *in vivo* settings. The applicability of *in vitro* estimates to *in*

vivo settings may not be quantitative, although proportionality has been suggested[40]. To test this here, we

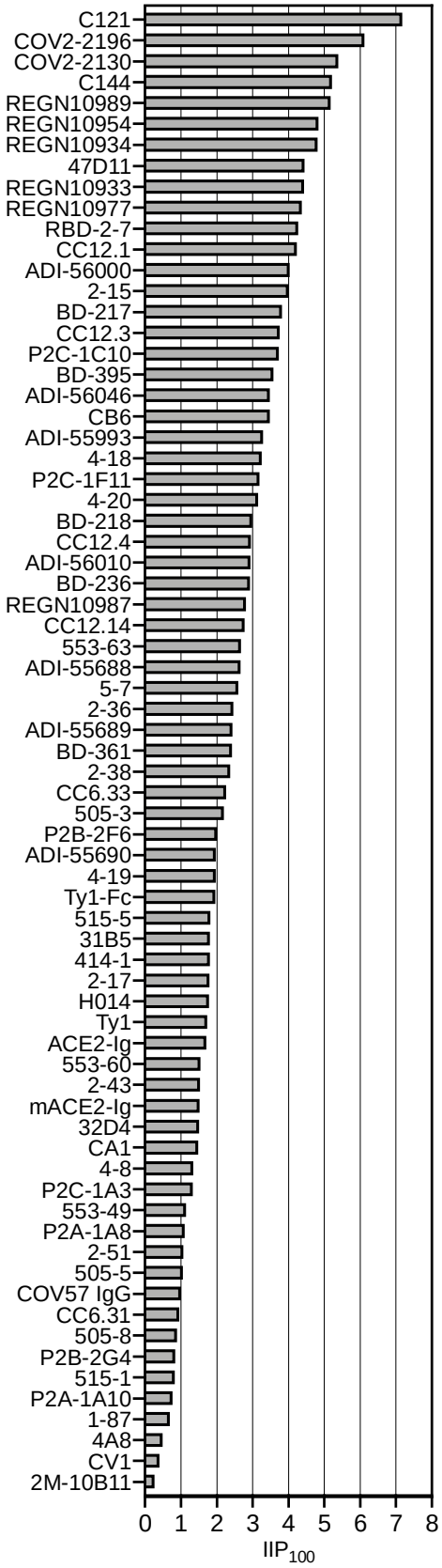

Figure 5. Comparison of SARS-CoV-2 NAbs based on *IIP*. A rank-order of SARS-CoV-2 NAbs based on *IIP* computed at 100 µg/ml. Average *IIP* is reported for 8 NAbs that have multiple neutralisation curves (Table S1).

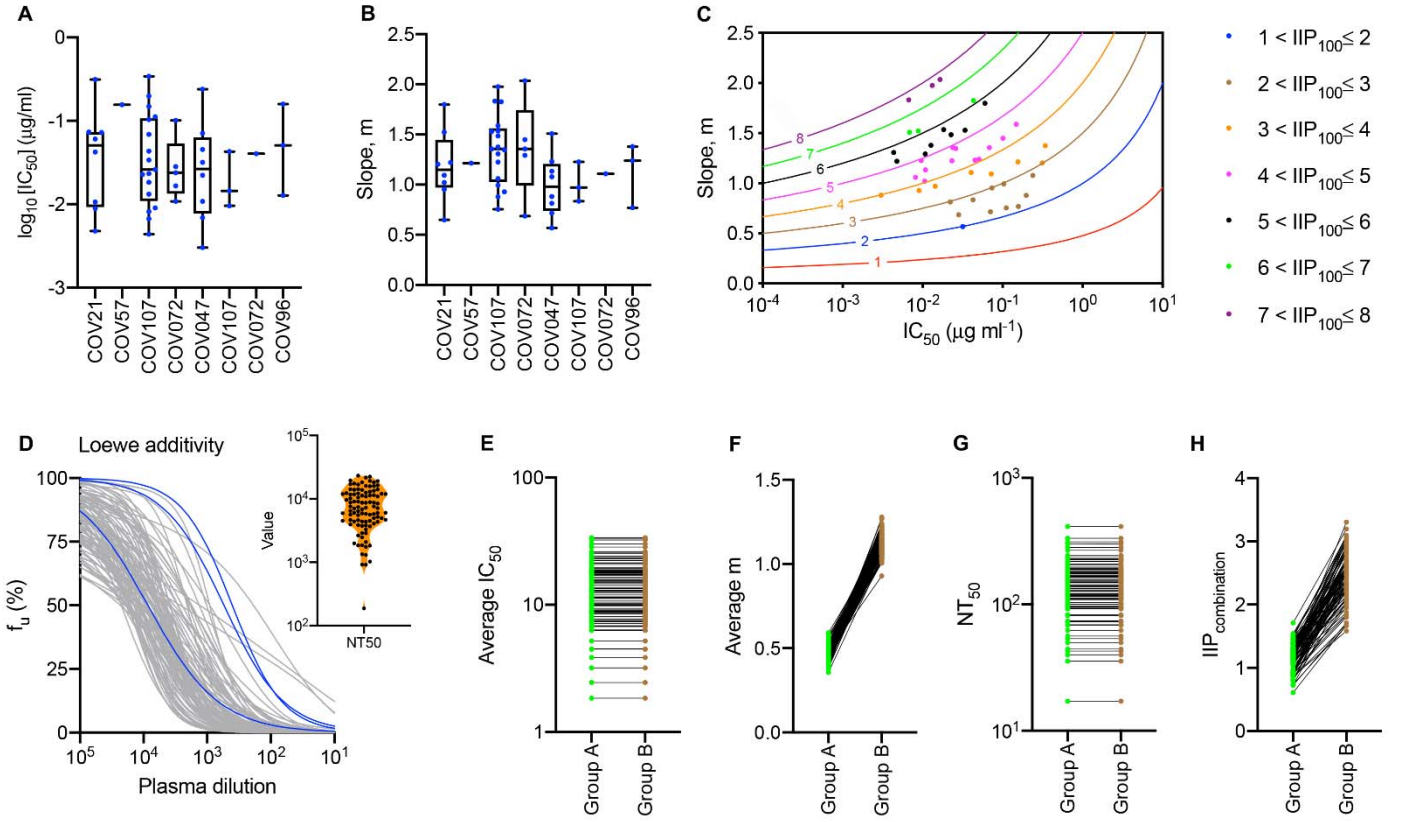

Figure 6. Applicability of the NAb landscape *in vivo*. (A, B) The variability in IC_{50} and m of different NAbs from eight patients (see Fig S8). The m values of NAbs with $IC_{50} \geq 1$ µg/ml could not be estimated and these NAbs are not shown. (C) IC_{50} and m for SARS-CoV-2 NAbs isolated from patients (circles colour-coded with the respective IIP values computed at 100 µg/ml). Each symbol represents one NAb. Contour lines represent loci of constant *IIP*. (D) Predictions (grey lines) of the fraction of infection events unaffected by NAbs, f_u, in the presence of increasing concentrations of plasma derived from virtual patients. We assumed ten NAbs per patient. IC_{50} for each NAb was sampled from the range 0.001 and 100 µg/ml and m from the range 0.2 and 2. Blues lines are fits to published data from three representative patients (see Fig. S8). *Inset*: half-maximal inhibitory plasma neutralizing titre, NT_{50}, values corresponding to the dilution curves in D. (E-H) Predictions of dilution curves of hypothetical patient plasma samples. (E, F) Average IC_{50} (E) and m (F) of groups A and B. (G, H) Comparison of NT_{50} (G) and *IIP* (H) between groups A and B. In D-H, D_0 = 100 µg/ml.

examined the spectrum of NAb responses reported within individual patients and compared them with the landscape. We considered reported DRCs of different NAbs from eight

patients[24] and estimated the corresponding IC_{50} and m (Figs. 6A, 6B, S7). We found the ranges of IC_{50} and m within each patient to be similar to the ranges in our landscape. For instance, in the patient COV021[24], the IC_{50} range was ~$5x10^{-3}$ to >1 µg/ml and the m values were in the range ~0.65 to 1.8. (Inhibition assays were not performed at NAb concentrations above 1 µg/ml, precluding analysis of NAbs with IC_{50}>1 µg/ml, of which there were several[24]. Such NAbs, expected to have low *IIP* values, are therefore missing in our landscape.) Similarly, in patient COV047, the IC_{50} range was ~$3x10^{-3}$ to >1 µg/ml and the m values were in the range ~0.6 to 1.5. In comparison, recall that the corresponding ranges were ~10^{-3} to 140 µg/ml and ~0.2 to 2.3 in the NAb landscape (Figs. 3, 4). We next computed *IIPs* of all of these NAbs and found them to lie in the range of 1 to 8, again in consonance with the landscape (Figs. 6C, 4A). These comparisons suggest that our landscape was representative of the spectrum of NAb responses within individuals.

To test this further, we performed *in silico* simulations that mimic plasma dilution assays used to quantify the antiviral efficacy of convalescent patient plasma samples (Fig. 6D). We assumed that the plasma samples contained 10 different NAbs with each NAb defined by its IC_{50} and m. We created *in silico* virtual patient plasma samples by randomly selecting IC_{50} and m for each of the 10 NAbs from the ranges identified from our landscape (Fig. 4). We assumed Loewe additivity[41-43] between the different NAbs to describe their overall efficacy. We found that with these *in silico* samples, we were able to closely recapitulate experimental serial dilution assays (Figs. 6D, S8), giving us confidence in the NAb landscape. The values of NT_{50}, the dilution at which neutralization efficiency decreases

by 50% of the undiluted plasma, we estimated (Fig. 5D inset) were also comparable to the values estimated from patient samples (~10^1 to 10^4; see Ref. 24).

These comparisons also re-emphasize the need to choose NAbs or convalescent patient plasma for treatment based not only on the IC_{50} but also *m*. To elucidate this further, we repeated our *in silico* analysis by comparing simulated samples containing NAbs with similar IC_{50} values but low (group A) or high (group B) *m* (Fig. 6E, 6F). Although simulated plasma samples from groups A and B had similar NT_{50} (Fig. 6G), samples with high *m* on average had much higher values of IIP_{100} than those with low *m* (Fig. 6H). Thus, in interpreting plasma dilution assays and in designing plasma and NAb therapies, accounting for *m*, which has been ignored thus far, would be as important as IC_{50}.

Discussion

Our study presents the first quantitative landscape of the NAb responses to SARS-COV-2. We deduced the landscape by the analysis of reported data from over 70 NAbs, which we collated into an extensive and mineable compendium. Importantly, the landscape recapitulated the spectrum of NAb responses seen in convalescent patients. We also rank-ordered the NAbs based on their *IIPs*, identifying promising candidates for further development, and setting benchmarks for NAbs that may be identified in the future.

An intriguing question that emerges is the nature of the NAbs that display high *IIP* values. Correlations have been proposed between the binding affinity of antibodies for their targets and the resulting neutralization efficiency, typically IC_{50}[44,45]. The origins of *m* are much less explored. Cooperative effects have been argued to lead to high *m*[46]. With SARS-

CoV-2, these effects are yet to be elucidated. In many cases, the targets and/or the mechanism of action of the NAbs are not known. For instance, the potent NAb 47D11 targeting the spike protein S of SARS-CoV-2 blocks virus entry without preventing the binding between S and the host receptor ACE-2 required for entry[32]. As future studies establish molecular details of the SARS-CoV-2 entry process[37,47], identifying unifying characteristics of the NAbs with high *IIP* values would become feasible, allowing rational design of even more potent NAbs.

Our analysis used data from pseudovirus assays because of the ease of interpretation of the assays and the known correlation of the *IIP* thus estimated with *in vivo* efficacy[48]. Analysis of assays using authentic SARS-CoV-2 virus, which would establish our findings on firmer footing, are not forthcoming. *m* is difficult to estimate using data from multi-round infection assays[49]. Further, viral kinetic parameters introduce confounding effects that are not readily delineated[49,50], posing challenges that extend beyond SARS-CoV-2. Nonetheless, the ability of our NAb landscape to recapitulate patient NAb responses and plasma dilution assays suggests that our findings are likely to be consistent with the scenario *in vivo*. Our aim is not to offer accurate estimates of the *in vivo* potency of NAbs. Rather, it is to present a systematic way of comparatively evaluating NAbs for further development and a benchmark for new NAbs.

In summary, our study collates, compares, and ranks available NAbs, laying out the landscape of NAb responses currently observed including in patients, and informs ongoing efforts to develop NAb-based interventions for SARS-CoV-2 infection.

Methods

Data

We considered data from studies that reported dose-response curves of NAbs using SARS-CoV-2 pseudotyped virions[21-39]. The assays estimate the fraction of infection events unaffected by the NAbs as a function of the NAb concentration (Fig. 2). Data from such assays have been successfully used to evaluate m and IC_{50} of antibodies against HIV-1[20] and HCV[18]. We extracted the data using Engauge Digitizer 12.1 and ensured consistency wherever possible with reported details, such as dilution levels used.

Analysis of DRCs

We used both the standard dose-response curve equation (Eq. [1]) and the median-effect equation (Eq. [2]) to analyse the data.

$$f_u = 1 - f_a = \frac{(IC_{50})^m}{(D)^m + (IC_{50})^m} \quad (1)$$

$$\log_{10}\left(\frac{f_a}{f_u}\right) = m\log_{10}\left(\frac{D}{IC_{50}}\right) \quad (2)$$

Here, f_u and f_a are the fraction of infection events unaffected and affected by the NAbs in a single round of infection, D is the NAb concentration, IC_{50} is the half-maximal inhibitory concentration and m is the slope. Data was fitted using the tool NLINFIT in MATLAB R2017b. Data points with 1% < f_u < 99% were considered for parameter estimation. We fit the data using Eq. [1] and Eq. [2] separately and obtained estimates of IC_{50} and m for each NAb as well as associated 95% confidence intervals. We then computed

$IIP_{100} = \log_{10}\left(1+\left(\frac{100}{IC_{50}}\right)^{m}\right)$ using the estimates obtained using Eq. [1] and Eq. [2]. In most cases, the IIP_{100} values were close to each other. We did not include NAbs for which IIP_{100} values estimated using the two methods deviated by 20% or more in our analysis, for the deviation indicated that such NAbs either did not conform to the trends expected by Eqs. [1] and [2] or had large uncertainties in the data precluding robust parameter estimation. We also repeated our analysis with a more liberal threshold of 30% deviation for acceptance (Fig. S9). The details of the NAbs and parameter estimates are presented in Table S1.

In silico simulation of plasma dilution assays

We simulated plasma dilution experiments as follows. We assumed that the plasma contained N NAbs with equimolar concentrations. For each NAb, IC_{50} was sampled from the range 0.001 µg/ml to 100 µg/ml (Fig. 3C) and m was sampled from the range 0.2 to 2 (Fig. 3D). This range was consistent with the range seen from the spectrum of NAbs within individual patients (Fig. 6A). The reciprocal plasma dilution curve was predicted assuming Loewe additivity between the different NAbs[41,42] using

$$\sum_{i=1}^{N}\frac{D_i/\gamma}{IC_{50_i}\left(\frac{1}{\varepsilon}-1\right)^{-1/m_i}}=1 \qquad (3)$$

Here, γ is the plasma dilution factor. ε is the fraction of infection events affected by the plasma in a single round of infection. D_i is the concentration of the i^{th} NAb in the plasma before dilution, IC_{50_i} is its half-maximal inhibitory concentration and m_i its slope, with

$i \in \{1,2,..,N\}$. We assumed N = 10 in our simulations, based on the number of NAbs with significant neutralization efficacy seen in patients[25]. We estimated the value of γ at which $\varepsilon = 0.5$ as the corresponding NT_{50}. We chose D_i as D_0 /N, and set D_0 = 100 µg/ml.

We repeated these simulations 100 times, with each simulation representative of an individual patient. We compared the resulting predictions with observations from 3 patients[51], which also we digitized (Fig. S8). The equation $f_u = \frac{(\gamma)^m}{(\gamma)^m + (NT_{50})^m}$ was fit to the observations from 3 patients. Here, m is the slope parameter, $\gamma$is the plasma dilution and NT_{50} is the half-maximal inhibitory plasma neutralizing titre. We also performed simulations where the IC_{50} values were kept similar between pairs of realizations, but m values were chosen from non-overlapping ranges. Using these simulations, we predicted how the expected plasma dilution assay data and the corresponding *IIP* values would vary with m.

Acknowledgements

This work was supported by the DBT/Wellcome Trust India Alliance Senior Fellowship IA/S/14/1/501307 to NMD.

Conflicting interests

The authors declare that no conflicts of interests exist.

References

1. Kelley, B. Developing therapeutic monoclonal antibodies at pandemic pace. *Nat Biotechnol* **38**, 540-545 (2020).

2. Renn, A., Fu, Y., Hu, X., Hall, M.D. & Simeonov, A. Fruitful Neutralizing Antibody Pipeline Brings Hope To Defeat SARS-Cov-2. *Trends Pharmacol Sci* (2020).

3. Yang, L., *et al.* COVID-19 antibody therapeutics tracker: a global online database of antibody therapeutics for the prevention and treatment of COVID-19. *Antibody Therapeutics* **3**, 204-211 (2020).

4. Focosi, D., Anderson, A.O., Tang, J.W. & Tuccori, M. Convalescent Plasma Therapy for COVID-19: State of the Art. *Clin Microbiol Rev* **33**, e00072-00020 (2020).

5. Chen, L., Xiong, J., Bao, L. & Shi, Y. Convalescent plasma as a potential therapy for COVID-19. *Lancet Infect Dis* **20**, 398-400 (2020).

6. Duan, K., *et al.* Effectiveness of convalescent plasma therapy in severe COVID-19 patients. *Proc Natl Acad Sci U S A* **117**, 9490-9496 (2020).

7. Abraham, J. Passive antibody therapy in COVID-19. *Nat Rev Immunol* **20**, 401-403 (2020).

8. Walker, L.M. & Burton, D.R. Passive immunotherapy of viral infections: 'super-antibodies' enter the fray. *Nat Rev Immunol* **18**, 297-308 (2018).

9. Caskey, M., Klein, F. & Nussenzweig, M.C. Broadly neutralizing anti-HIV-1 monoclonal antibodies in the clinic. *Nat Med* **25**, 547-553 (2019).

10. Beck, A., Wurch, T., Bailly, C. & Corvaia, N. Strategies and challenges for the next generation of therapeutic antibodies. *Nat Rev Immunol* **10**, 345-352 (2010).

11. Chan, A.C. & Carter, P.J. Therapeutic antibodies for autoimmunity and inflammation. *Nat Rev Immunol* **10**, 301-316 (2010).

12. Scott, A.M., Wolchok, J.D. & Old, L.J. Antibody therapy of cancer. *Nat Rev Cancer* **12**, 278-287 (2012).

13. Sliwkowski, M.X. & Mellman, I. Antibody therapeutics in cancer. *Science* **341**, 1192-1198 (2013).

14. Shen, L., *et al.* Dose-response curve slope sets class-specific limits on inhibitory potential of anti-HIV drugs. *Nat Med* **14**, 762-766 (2008).

15. Jilek, B.L., *et al.* A quantitative basis for antiretroviral therapy for HIV-1 infection. *Nat Med* **18**, 446-451 (2012).

16. Sampah, M.E., Shen, L., Jilek, B.L. & Siliciano, R.F. Dose-response curve slope is a missing dimension in the analysis of HIV-1 drug resistance. *Proc Natl Acad Sci U S A* **108**, 7613-7618 (2011).

17. Laskey, S.B. & Siliciano, R.F. Quantitative evaluation of the antiretroviral efficacy of dolutegravir. *JCI Insight* **1**, e90033 (2016).

18. Padmanabhan, P. & Dixit, N.M. Inhibitors of hepatitis C virus entry may be potent ingredients of optimal drug combinations. *Proc Natl Acad Sci U S A* **114**, E4524-E4526 (2017).

19. Koizumi, Y., *et al.* Quantifying antiviral activity optimizes drug combinations against hepatitis C virus infection. *Proc Natl Acad Sci U S A* **114**, 1922-1927 (2017).

20. Webb, N.E., Montefiori, D.C. & Lee, B. Dose-response curve slope helps predict therapeutic potency and breadth of HIV broadly neutralizing antibodies. *Nat Commun* **6**, 8443 (2015).

21. Seydoux, E., *et al.* Analysis of a SARS-CoV-2-Infected Individual Reveals Development of Potent Neutralizing Antibodies with Limited Somatic Mutation. *Immunity* **53**, 98-105 e105 (2020).

22. Zost, S.J., *et al.* Potently neutralizing and protective human antibodies against SARS-CoV-2. *Nature* **584**, 443-449 (2020).

23. Wan, J., *et al.* Human-IgG-Neutralizing Monoclonal Antibodies Block the SARS-CoV-2 Infection. *Cell Rep* **32**, 107918 (2020).

24. Robbiani, D.F., *et al.* Convergent antibody responses to SARS-CoV-2 in convalescent individuals. *Nature* **584**, 437-442 (2020).

25. Liu, L., *et al.* Potent neutralizing antibodies against multiple epitopes on SARS-CoV-2 spike. *Nature* **584**, 450-456 (2020).

26. Chi, X., *et al.* A neutralizing human antibody binds to the N-terminal domain of the Spike protein of SARS-CoV-2. *Science* **369**, 650-655 (2020).

27. Hansen, J., *et al.* Studies in humanized mice and convalescent humans yield a SARS-CoV-2 antibody cocktail. *Science* **369**, 1010-1014 (2020).

28. Ju, B., *et al.* Human neutralizing antibodies elicited by SARS-CoV-2 infection. *Nature* **584**, 115-119 (2020).

29. Lei, C., *et al.* Neutralization of SARS-CoV-2 spike pseudotyped virus by recombinant ACE2-Ig. *Nat Commun* **11**, 2070 (2020).

30. Shi, R., *et al.* A human neutralizing antibody targets the receptor-binding site of SARS-CoV-2. *Nature* **584**, 120-124 (2020).

31. Cao, Y., *et al.* Potent Neutralizing Antibodies against SARS-CoV-2 Identified by High-Throughput Single-Cell Sequencing of Convalescent Patients' B Cells. *Cell* **182**, 73-84 e16 (2020).

32. Wang, C., *et al.* A human monoclonal antibody blocking SARS-CoV-2 infection. *Nat Commun* **11**, 2251 (2020).

33. Chen, X., *et al.* Human monoclonal antibodies block the binding of SARS-CoV-2 spike protein to angiotensin converting enzyme 2 receptor. *Cell Mol Immunol* **17**, 647-649 (2020).

34. Lv, Z., *et al.* Structural basis for neutralization of SARS-CoV-2 and SARS-CoV by a potent therapeutic antibody. *Science* **369**, 1505-1509 (2020).

35. Rogers, T.F., *et al.* Isolation of potent SARS-CoV-2 neutralizing antibodies and protection from disease in a small animal model. *Science* **369**, 956-963 (2020).

36. Wec, A.Z., *et al.* Broad neutralization of SARS-related viruses by human monoclonal antibodies. *Science* **369**, 731-736 (2020).

37. Barnes, C.O., *et al.* Structures of Human Antibodies Bound to SARS-CoV-2 Spike Reveal Common Epitopes and Recurrent Features of Antibodies. *Cell* **182**, 828-842 e816 (2020).

38. Pinto, D., *et al.* Cross-neutralization of SARS-CoV-2 by a human monoclonal SARS-CoV antibody. *Nature* **583**, 290-295 (2020).

39. Hanke, L., *et al.* An alpaca nanobody neutralizes SARS-CoV-2 by blocking receptor interaction. *Nat Commun* **11**, 4420 (2020).

40. van Gils, M.J. & Sanders, R.W. In vivo protection by broadly neutralizing HIV antibodies. *Trends Microbiol* **22**, 550-551 (2014).

41. Padmanabhan, P. & Dixit, N.M. Modeling Suggests a Mechanism of Synergy Between Hepatitis C Virus Entry Inhibitors and Drugs of Other Classes. *CPT Pharmacometrics Syst Pharmacol* **4**, 445-453 (2015).

42. Chou, T.C. Theoretical basis, experimental design, and computerized simulation of synergism and antagonism in drug combination studies. *Pharmacol Rev* **58**, 621-681 (2006).

43. Foucquier, J. & Guedj, M. Analysis of drug combinations: current methodological landscape. *Pharmacol Res Perspect* **3**, e00149 (2015).

44. Liao, H.X., *et al.* Co-evolution of a broadly neutralizing HIV-1 antibody and founder virus. *Nature* **496**, 469-476 (2013).

45. Bonsignori, M., *et al.* Maturation Pathway from Germline to Broad HIV-1 Neutralizer of a CD4-Mimic Antibody. *Cell* **165**, 449-463 (2016).

46. Shen, L., *et al.* A critical subset model provides a conceptual basis for the high antiviral activity of major HIV drugs. *Sci Transl Med* **3**, 91ra63 (2011).

47. Wang, Y., Liu, M. & Gao, J. Enhanced receptor binding of SARS-CoV-2 through networks of hydrogen-bonding and hydrophobic interactions. *Proc Natl Acad Sci U S A* **117**, 13967-13974 (2020).

48. Rosenbloom, D.I., Hill, A.L., Rabi, S.A., Siliciano, R.F. & Nowak, M.A. Antiretroviral dynamics determines HIV evolution and predicts therapy outcome. *Nat Med* **18**, 1378-1385 (2012).

49. Ferguson, N.M., Fraser, C. & Anderson, R.M. Viral dynamics and anti-viral pharmacodynamics: rethinking in vitro measures of drug potency. *Trends Pharmacol Sci* **22**, 97-100 (2001).

50. Padmanabhan, P. & Dixit, N.M. Mathematical model of viral kinetics in vitro estimates the number of E2-CD81 complexes necessary for hepatitis C virus entry. *PLoS Comput Biol* **7**, e1002307 (2011).

51. Brouwer, P.J.M., *et al.* Potent neutralizing antibodies from COVID-19 patients define multiple targets of vulnerability. *Science* **369**, 643-650 (2020).